Poly(propylene fumarate) Bone Tissue Engineering Scaffold Fabrication Using Stereolithography: Effects of Resin Formulations and Laser Parameters

Kee-Won Lee,[†,‡] Shanfeng Wang,[†,‡] Bradley C. Fox,[†] Erik L. Ritman,[‡] Michael J. Yaszemski,[†,‡] and Lichun Lu*[,†,‡]

Departments of Orthopedic Surgery and Biomedical Engineering, Mayo Clinic College of Medicine, 200 First Street SW, Rochester, Minnesota 55905

Received August 28, 2006; Revised Manuscript Received December 11, 2006

Stereolithography using photo-cross-linkable polymeric biomaterials is an effective technique for fabricating highly complex three-dimensional (3D) scaffolds with controlled microstructures for tissue engineering applications. In this study, we have optimized the UV curable polymer solution composition and laser parameters for the stereolithography machine. Poly(propylene fumarate) (PPF) was used as the biomaterial, diethyl fumarate (DEF) was used as the solvent, and bisacrylphosphrine oxide (BAPO) was used as the photoinitiator. Three different weight ratios of PPF/DEF and BAPO contents were characterized by measuring the viscosities and thermal properties of the un-cross-linked solutions and the mechanical properties of the formed scaffolds. After optimizing the resin composition by satisfying both the viscosity limitation and the mechanical requirement, laser parameters such as critical exposure (E_c) and penetration depth (D_p) were determined from the working curve and the relationship between laser speed and energy by measuring the thickness of predesigned windows fabricated in stereolithography with different ranges of E_c and D_p. Three-dimensional scaffolds with various pore sizes, pore shapes, and porosities were designed in computer-aided design (CAD) software and were fabricated in stereolithography. The fabricated scaffolds were characterized by measuring external dimensions, porosities, mean pore sizes, and compressive moduli and were compared to the CAD models. Feature accuracy in the *xy*-plane was achieved and overcuring of the resin in *z*-axis was minimized. The stereolithographically fabricated scaffolds with controlled microstructures can be useful in diverse tissue engineering applications.

Introduction

Biodegradable polymers are attractive as scaffold materials for bone tissue engineering because of good processibility. Their properties may be controlled to satisfy specific design requirements such as biocompatibility, biodegradability, highly porous and well-interconnected structure, high surface area to volume ratio, appropriate surface chemistry, and mechanical properties.[1,2]

Scaffold properties depend not only on the intrinsic properties of biomaterial but also on the fabrication process. Solid freeform fabrication (SFF) has the potential of fabricating complex three-dimensional (3D) structures with controlled microstructures because it uses computer-aided design (CAD).[3] Among the various SFF techniques available, stereolithography is a widely used technique that fabricates 3D structures layer-by-layer by polymerizing photo-cross-linkable liquid resin using a small-sized laser beam.[4−6] This technique has been successfully applied to fabricate biomimetic scaffolds from imaging modalities[7−10] or predesigned scaffolds by using photo-cross-linkable materials.[11,12]

Most materials used for stereolithography are conventional epoxy resins, thermoplastic elastomers, and poly(ethylene glycol) (PEG)-based hydrogels. They have limited application in bone tissue engineering because of the lack of biodegradability or sufficient mechanical strength. One promising material to overcome these limitations is poly(propylene fumarate) (PPF), an unsaturated linear polyester that can be cross-linked though its carbon−carbon double bonds[13] and can be degraded by simple hydrolysis of the ester bonds into nontoxic products.[14] PPF has been used as an injectable[15,16] material for making preformed scaffolds for bone tissue engineering applications though chemical- or photo-cross-linking in combination with the salt leaching technique.[17−19] Recently, stereolithography was used to fabricate a 3D prototype for critical-sized defect repair by using PPF/DEF resin mixed with a photoinitiator, bisacrylphosphrine oxide (BAPO).[20,21] Although these studies showed the feasibility of fabricating 3D prototypes in stereolithography, optimal PPF/DEF resin and laser parameters for building 3D scaffolds with controlled microstructures in a conventional stereolithography machine have not yet been investigated.

The objective of this study was to obtain optimal UV curable polymer resin composition and laser parameters for a conventional stereolithography machine to fabricate 3D scaffolds with controlled microstructures specifically for bone tissue engineering applications. PPF/DEF mixtures with three different weight ratios and BAPO contents were investigated. The viscosities and thermal properties of the un-cross-linked solutions and the mechanical properties of the final cross-linked samples were determined. Laser parameters for the selected resin were obtained by measuring the thickness of predesigned windows fabricated in stereolithography with different ranges of critical exposure (E_c) and penetration depth (D_p) and by obtaining the working curve and the relationship between laser speed and

* To whom correspondence should be addressed. Tel: (507) 284-2267; fax: (507) 284-5075; e-mail: lu.lichun@mayo.edu.

† Department of Orthopedic Surgery.

‡ Department of Physiology and Biomedical Engineering.

10.1021/bm060834v CCC: $37.00
Published on Web 02/28/2007

energy. 3D orthogonal cubic-lattice disk scaffolds with various pore sizes, pore shapes, and porosities were designed in CAD software. Stereolithographically fabricated scaffolds were characterized by measuring external dimension, porosity from gravimetric analysis and microcomputed tomography (micro-CT), surface pore morphology and mean pore size from scanning electron microscopy (SEM), and mechanical properties from compression testing using a dynamic mechanical analyzer (DMA).

Experimental Section

PPF Synthesis. As described previously,[22,23] DEF and excess amount of 1,2-propylene glycol were polymerized together with hydroquinone (cross-linking inhibitor) and zinc chloride (catalyst) first at 100 °C for 1 h and then at 150 °C for 7 h to get the intermediate dimer. The intermediate dimer was polymerized to PPF via condensation under vacuum at 130 °C for another 4 h. Gel permeation chromatography (GPC) was used to determine the molecular weight and polydispersity of PPF. The GPC was carried out with a Waters 717 Plus Autosampler GPC system (Waters, Milford, MA) connected to a model 515 HPLC pump and model 2410 refractive index detector. Monodispersed polystyrene standards (Polysciences, Warrington, PA) with number-average molecular weights (M_n) of 889, 2790, and 10400 g/mol were used to construct the calibration curve. The M_n and weight-average molecular weight (M_w) of the synthesized PPF were 2016 and 3413 g/mol, respectively.

PPF/DEF Resin Preparation. UV curable resin was prepared by dissolving PPF in DEF at 37 °C for 24 h and by mixing the PPF/DEF solution with bisacrylphosphrine oxide (BAPO, Ciba Specialty Chemicals, Tarrytown, NY), the photoinitiator. Three different weight ratios of PPF:DEF (75:25, 60:40, and 50:50) and BAPO contents (0.1, 0.5, and 1 wt % of PPF/DEF solution) were used to investigate the effects of formulations on fabrication and the mechanical properties of the 3D scaffolds prepared using stereolithography.

Resin Characterization. Differential scanning calorimetry (DSC) was measured on a TA Instruments Q1000 differential scanning calorimeter at a heating rate of 10 °C/min in a nitrogen atmosphere. Each sample was preheated from room temperature to 100 °C and was cooled to −90 °C at a cooling rate of 5 °C/min. Then, the DSC scan was recorded via heating from −90 to 100 °C. Thermogravimetric analysis (TGA) was done using a TA Instruments Q500 thermal analyst. The TGA data were obtained in flowing nitrogen at a heating rate of 20 °C/min. Linear viscoelastic properties of PPF and PPF/DEF solutions were measured on a rheometer (AR2000, TA instruments, New Castle, DE) in a frequency range of 0.5−628.3 rad/s at 25 °C. Oscillatory shear measurements were carried out using a 20-mm-diameter parallel plate flow cell with a geometry gap of 1.0 mm to measure the zero-shear viscosity η_0. No strain amplitudes were greater than 10%.

Laser Parameter Determination. Windows used for determining laser parameters of the resin were designed in CAD software, SolidWorks (SolidWorks Corp., Concord, MA), which had a length and width of 0.5 cm and a height of 0.1 cm. After converting these CAD files to stereolithography files, 2D sliced data (BFF) file was made with 101.6-μm (=0.004 in.) layer thickness and no supports in 3D Lightyear software. The number of up, down, and layer hatches was set at 1, and all other hatch and border overcures were set at 0.01 as the maximum value. One single layer of three windows was cured at a time from the PPF/DEF resin poured into a Petri dish in the Viper si2 stereolithography system (3D systems, Valencia, CA). Different ranges of E_c (5−12 mJ/cm^2) and D_p (1−5 mil) were applied. Mil is a unit of length equal to one thousandth of an inch (0.0254 mm). After removing excess resin and postcuring for 30 min, the thickness of one single layer in each window was measured using an electrical caliper, and energy (E) was calculated from the equation $E = [P_L/(W_o \times V_s)] \times [2/\pi]^{1/2}$, where P_L is the laser power, W_o is the laser beam diameter (=250 μm), and V_s is the laser speed.[27] Using these values, the working curve of resin was obtained by plotting a semilogarithmic graph between energy and thickness. E_c and D_p were determined as the x-intercept (=ln(E_c)) and the slope of the working cure, respectively.

Scaffold Design in CAD. The CAD designed scaffolds were orthogonal cubic-lattice disks with square or hexagon pores. The external dimensions were 1 cm in length, 1 cm in width, and 0.3 cm in thickness, and the strut thickness was 300 μm. Using these fixed parameters, pore size and porosity of each scaffold were calculated. For the scaffolds with square pores, the range of pore sizes was approximately from 400 μm to 1 mm, whereas for those with hexagon pores, the length of one side of pore was 600 μm. The pore sizes and porosities of CAD models are shown in Table 2.

Scaffold Fabrication in Stereolithography. All CAD files were converted to STL files which were then used to design supports and 2D sliced data (BFF) file with 101.6-μm (=0.004 in.) layer thickness in 3D Lightyear software. BFF files were imported to the Viper si2 stereolithography system for fabricating 3D scaffolds by photo-cross-linking PPF resins layer-by-layer with UV laser. After fabrication, supports were removed carefully with a razor blade and scaffolds were rinsed with 100% ethanol several times to remove excess resin trapped inside. In the final step, scaffolds were dried completely at room temperature and were postcured in a UV oven for 2 h. All the scaffolds were fabricated at the same time using the same batch of PPF. The scheme and fabrication process of 3D scaffolds in stereolithography are shown in Figure 1a and 1c.

Scaffold Characterization. As described in Resin Characterization, the thermal properties of a cross-linked PPF sample taken from the scaffold with square pores (pore size = 670 μm, porosity = 49.1%) fabricated in stereolithography were also studied. Prior to thermal analysis, the sample was extracted in THF overnight on a Soxhlet extraction apparatus for separating sol and gel fractions. The gel fraction of the samples was calculated to be around 97.4% by weighing the samples before extraction and after drying. External dimensions (length, width, and height) and dry mass of PPF scaffolds were measured using a digital caliper and an electric balance, respectively. Dimensional difference between CAD models and fabricated scaffolds was calculated by $[(d_s - d_{CAD})/d_{CAD}] \times 100(\%)$, where d_{CAD} and d_s are the dimension of CAD models and PPF scaffolds, respectively. Porosity of PPF scaffolds was calculated by $[1 - (m_s/v_s)/\rho_{PPF}] \times 100(\%)$, where v_s is the total volume, m_s is the dry mass of PPF scaffold, and ρ_{PPF} is the density of PPF (~1.3 g/cm^3).[23]

Nondestructive, 3D images of the scaffold were obtained from the micro-CT system, custom-built in-house from commercially available components, and were described in detail previously.[24] Scaffolds were mounted on a rotary stage and were scanned in their entirety (approximately 160 mm^3) at 17 keV of peak emission X-rays, being rotated 360° in 361 equiangular steps. Each of these two-dimensional (2D) projections was deconvolved with its measured, spatially variant point spread function. All resulting images were reconstructed using a modified Feldkamp cone beam tomographic reconstruction algorithm[25] resulting in cubic voxels, which were 17.1 μm on each side. Images were segmented by an operator-selected threshold of intensities to separate voxels representing regions of differing density and then were analyzed to obtain volume fractions of each scaffold following the previous study.[26] Volume fractions of pore and polymer were obtained by selecting subregions of each volume representing a scaffold and by logging counts of voxels representing each material along the slices. These quantitative analyses were implemented using the biomedical image analysis software, Analyze (Biomedical Imaging Resources, Mayo Clinic, Rochester, MN).

Surface pore morphology of PPF scaffolds in the xy-plane and z-axis was examined by cold-field emission scanning electron microscopy (SEM) (S-4700, Hitachi Instruments Inc., Tokyo, Japan). All samples were viewed at 3 kV accelerating voltage and 9500 nA emission current. From SEM images, mean pore size of scaffolds was determined using Analyze software.

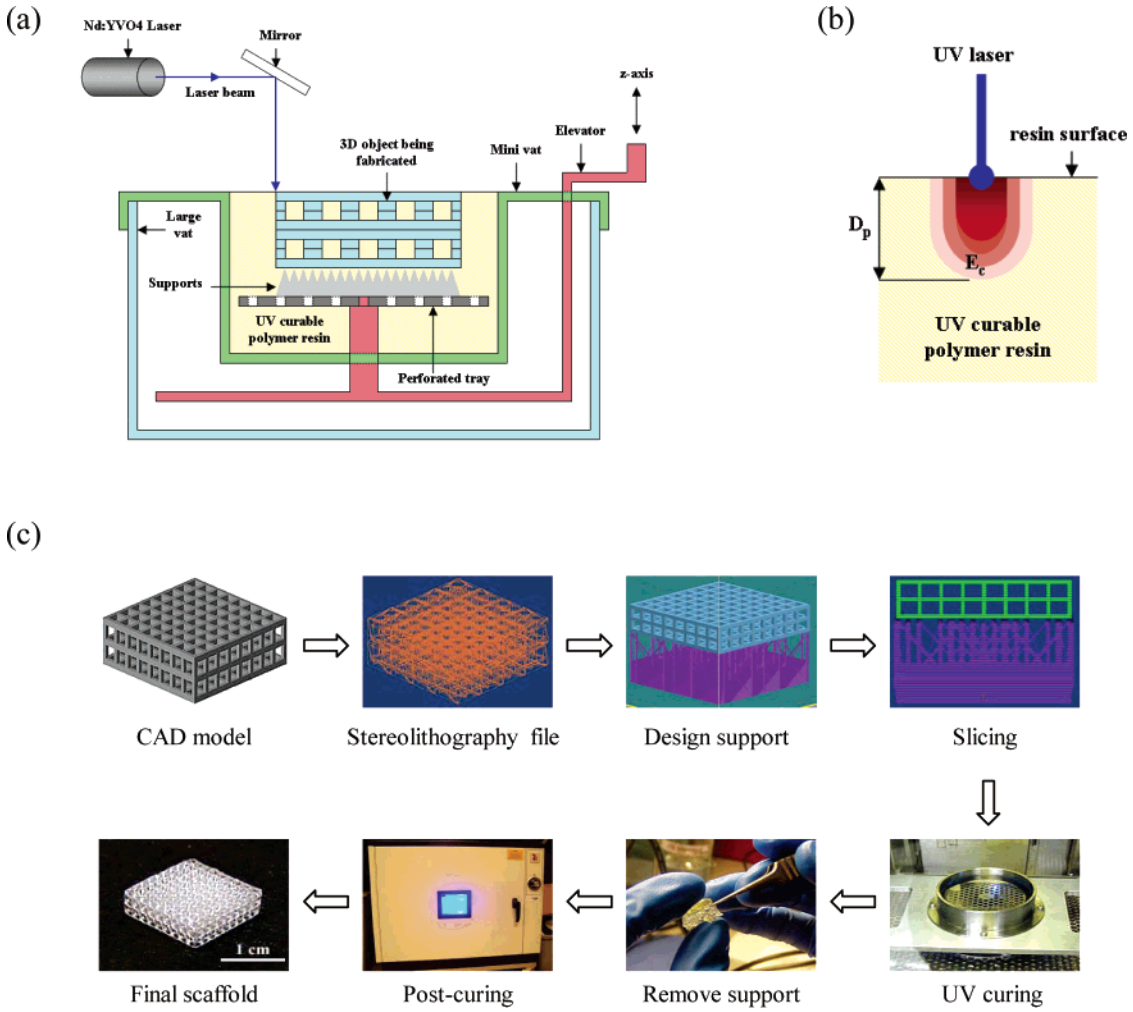

Figure 1. (a) Schematic of the stereolithography system, (b) UV laser parameters, and (c) fabrication process of 3D scaffolds by stereolithography.

Compression testing for UV curable resins with different formulations and fabricated scaffolds was implemented by a dynamic mechanical analyzer (DMA 2980, TA instruments). Cylindrical samples (4 mm in diameter by 8 mm in height) for three PPF/DEF weight ratios and BAPO contents were prepared in a glass mold using a UV lamp (B-100 AP, Blak-Ray Inc., Upland, CA) with a wavelength of 365 nm for 10 min. Before testing, initial cross section area and dimension of each sample were measured. All the samples were compressed at a rate of 1 mm/min. Compressive moduli were determined by dividing applied forces and dimensional changes into initial cross section area and height and then by calculating the slope of the first linear region after the initial rising portion in the stress/strain curve.

Statistical Analysis. All measured data were reported as means ± standard deviations for $n = 5$. Student's *t*-test was performed to assess statistically significances ($p < 0.05$) of external dimensions and porosities between CAD models and PPF scaffolds.

Results and Discussion

PPF/DEF mixtures with three different weight ratios and BAPO contents were investigated to obtain optimal UV curable resin for fabricating 3D scaffolds in the stereolithography. Preliminary data have shown that the PPF/DEF weight ratios between 50:50 and 75:25 are suitable for stereolithography to achieve scaffolds with variant mechanical strengths;[28] moreover, photo-cross-linking properties of the mixture are significantly influenced by molecular weight of PPF, DEF content, and BAPO content.[21] Since the same batch of PPF (M_n = 2016 g/mol) was used throughout this study, DEF and BAPO contents are focused to investigate their roles in affecting both cross-linking characteristics and physical properties of the final scaffolds.

There is a viscosity limitation for the resin used in stereolithography. In this study, PPF with a molecular weight of 2016 g/mol has a melt viscosity of 2.81×10^6 Pa·s. Therefore, it should be dissolved in a solvent such as DEF to allow scaffold fabrication. Besides reducing the viscosity of PPF, DEF can participate in cross-linking. When the composition of PPF in the PPF/DEF is lower than 50% at 0.5% of BAPO content, the mechanical properties of the formed scaffolds decreased sharply although the viscosity satisfied the fabrication requirements.[21] The PPF/DEF solutions with three compositions have been made and investigated in terms of thermal and mechanical properties together with PPF itself and cross-linked samples. As shown in the DSC curves in Figure 2a, the glass-transition temperature T_g drops dramatically from 12.5 °C for pure PPF to −41.4 °C when adding 25% DEF. When the composition of PPF decreases further, T_g continues to drop; however, the solutions start to show phase separation as indicated by multiple glass transitions in DSC curves. The sample from a photo-cross-linked scaffold does not show any glass transitions in the temperature range studied here since all the segmental motions are prohibited after cross-linking.

TGA curves in Figure 2b show a single thermal degradation step for pure PPF while two steps for PPF/DEF solutions and

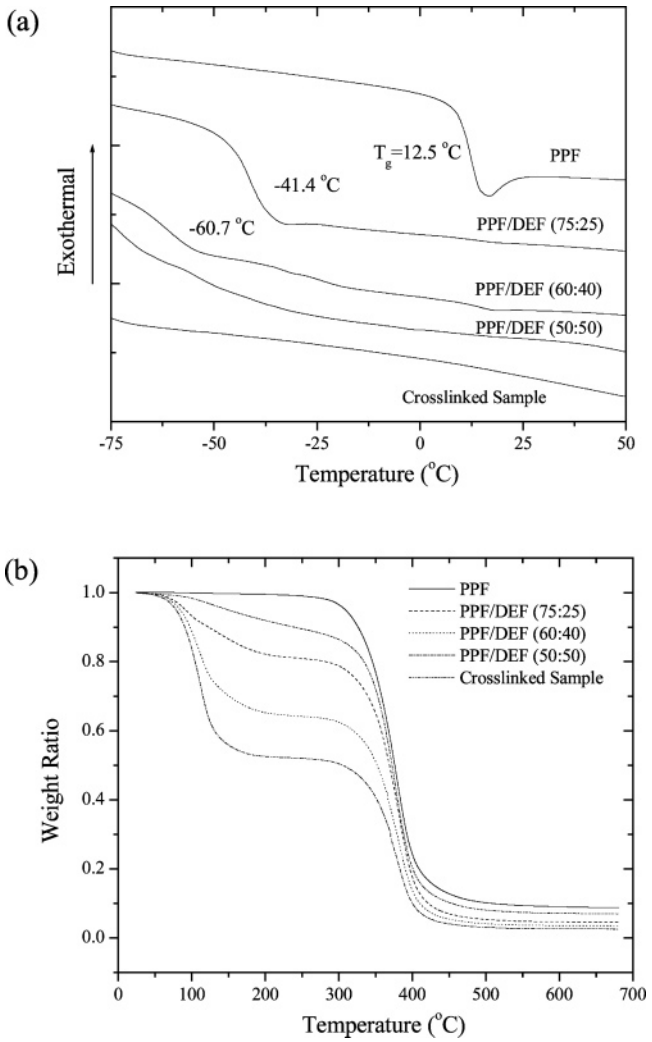

Figure 2. (a) DSC curves and (b) TGA thermograms of PPF/DEF solutions at various compositions and cross-linked samples formed using PPF/DEF resin.

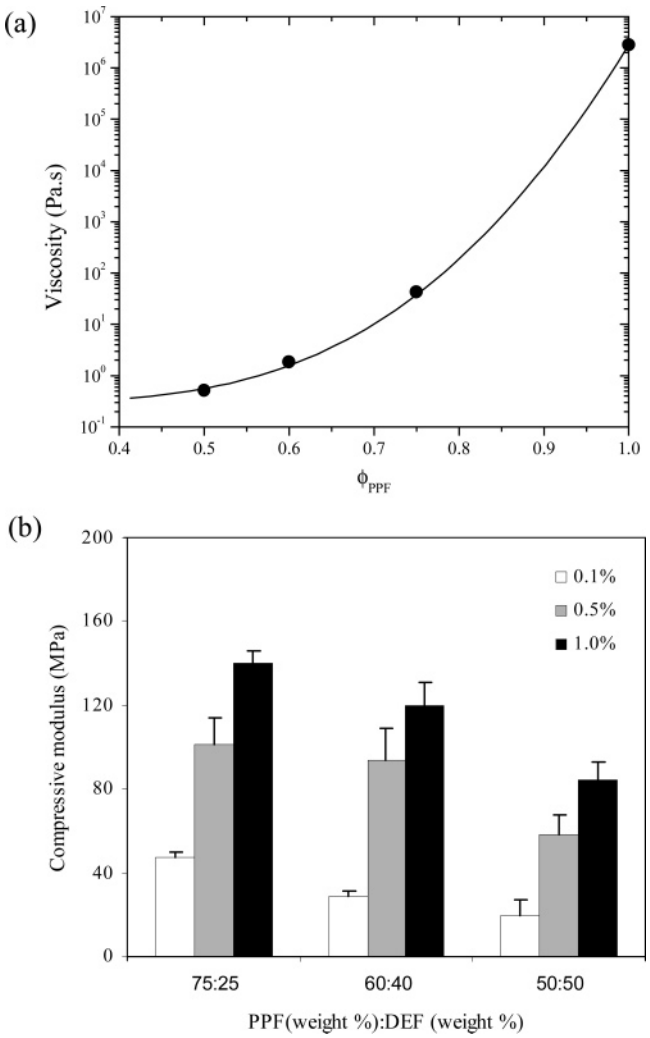

Figure 3. (a) Viscosity of un-cross-linked solution with various PPF/DEF weight ratios. (b) Compressive modulus of cylindrical samples fabricated from PPF/DEF resin with three different weight ratios and BAPO contents. Values represent mean ± SD ($n = 5$).

cross-linked scaffold. The thermal degradation temperature for PPF used in this study is around 338 °C. This temperature drops slightly with adding more DEF. Another degradation temperature appears around 80 °C for the samples containing DEF. The weight ratio for this degradation step is consistent with the corresponding composition of DEF; however, the deviation becomes significant when the composition of PPF is as high as 80% because a fraction of DEF participated in the thermal cross-linking during the heating process. The TGA curve for the cross-linked sample further verifies that DEF is a part of the cross-linked PPF network as a cross-linker while its fraction is only about 10 wt %, as revealed in the weight loss. The residue after thermal degradation decreased with decreasing the PPF composition.

The viscosity η of un-cross-linked PPF/DEF solutions at 25 °C decreased sharply from 2.81×10^6 to 0.51 Pa·s with increasing DEF content from 0 to 50% in Figure 3a. As also revealed in the previous study[29] and the decreased T_g shown in Figure 2a, both dilution and plasticization effects of DEF in the solution occurred because dilution effect alone could not render such a steep composition dependence.[30,31] In our previous study,[29] three different molecular weights of PPF have been investigated for the composition dependence of viscosity, and it has been observed that a lower PPF composition in PPF/DEF resin should be used to satisfy the viscosity limitation for a higher molecular weight. Meanwhile, it is anticipated that a higher molecular weight of PPF gives better mechanical properties after cross-linking at the same condition for the same PPF/DEF weight ratio. As a result, the molecular weight of PPF plays not only a direct role in determining the final scaffold's mechanical properties but also an indirect role in determining the highest possible polymer concentration one can use in stereolithography. To not sacrifice the mechanical properties, molecular weight of PPF should fall into a range to make the viscosity of PPF/DEF no larger than the required maximum when the concentration is approximately between 60% and 75%. Figure 3a suggests the PPF sample with an $M_n = 2016$ g/mol satisfies this criterion.

The increased viscosity of resin may lead to slow resin flows on the top of the build platform, which will increase fabrication time and make a convex mound on the surface of the building part after each recoating cycle.[20] Zephyr blade in stereolithography system is used to avoid this convex surface effect by moving the resin up to the elevator automatically when it lowers into the vat. However, for the custom-built minivat used in this study (Figure 1a), decreased resin viscosity is one of the major factors for determining fabrication time and feature accuracy in stereolithography. Considering that viscosities of the conventional solid-state epoxy resin ranged from 0.2 to 1.6 Pa·s at 30 °C, our results show that the DEF composition of 60%

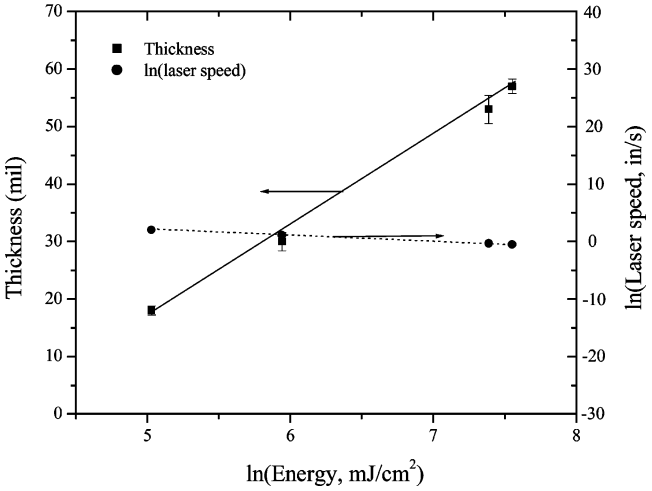

Figure 4. Effects of laser energy on the thickness of the building part and the laser speed. Energy and laser speed are plotted in logarithmic scale. Values represent mean ± SD ($n = 5$). Solid and dotted lines represent linear regression.

(viscosity = 1.8 Pa·s) may be the upper limit for PPF/DEF resin used here in stereolithography.

As shown in Figure 3b, the compressive modulus of the cylindrical samples fabricated from PPF/DEF resin was higher for less DEF content and more BAPO content. The compressive modulus ranges from 19 ± 7.8 to 140 ± 6.1 MPa. The maximum value was found in PPF/DEF resin with 75:25 weight ratios and 1% of BAPO content. As cited earlier, Fisher et al.[21] showed that roughly 25% DEF content was optimal for producing the highest elastic modulus and fracture strength. On the basis of the previously reported compressive modulus (50 ∼ 500 MPa)[32] of human trabecular bone, we suggest that DEF content (<50%) and BAPO content (>0.1%) be the optimal concentrations of PPF/DEF resin for bone tissue engineering applications. Therefore, we chose the PPF/DEF mixture with 60:40 weight ratio and 1% BAPO content as UV curable resin for stereolithography machine in later scaffold fabrication and related studies.

Laser parameters of the UV curable resin in stereolithography machine are indicated in Figure 1b. When a laser beam hits the resin surface, its energy is maximum at that spot and decreases when increasing width and depth in the *xy*-plane and *z*-axis, respectively. E_c and D_p are the two primary parameters of the resin itself, which are determined generally by windowpane analysis from the following equation: $C_d = D_p \cdot \ln(E_{max}/E_c)$, where C_d is the cure depth, and E_{max} is the maximum energy exposure.[27] The working curve and correlation between energy and laser speed of our resin are shown in Figure 4. One single layer of windows was not cured when the laser speed was more than 50 in./s. From this working curve, E_c and D_p were calculated as 48.1 mJ/cm^2 and 15.3 mil, respectively. After applying the E_c and D_p values to fabricate the window in stereolithography system, the border and hatch speed were 46.6 in./s and the thickness of one single layer in each window was 267.3 μm. Similar to the previous work,[28] this result shows that E_c and D_p for PPF/DEF resin could not be optimized by the windowpane analysis because the thicknesses of the individual windowpanes were outside the expected values (=101.6 μm). Since E_c and D_p affect both laser power and speed, to determine these two laser parameters, the required laser energy and speed for curing our layer thickness were calculated to be 62.5 mJ/cm^2 from the working curve and 10.6 in./s from the graph of laser speed against energy. Finally, E_c and D_p for satisfying calculated laser energy and speed were determined as 10 mJ/cm^2 and 3.66 mil, respectively.

Orthogonal cubic-lattice scaffolds with various pore sizes and porosities were designed using CAD software. The ranges of pore sizes and porosities for CAD models were 446−913 μm and 55.4−79.5%, respectively (Table 2). In scaffolds with hexagon pores, an actual pore size of 1.2 mm was designed as the maximum diagonal length. We fixed the strut thickness of scaffolds as 300 μm, considering that the laser beam diameter was 250 μm in stereolithography machine, which is the critical machine-specific parameter for determining resolution of feature.[4] These pore sizes have been investigated as optimal pore sizes in bone tissue engineering because they had a greater influence on bone ingrowth and vascularization in vivo.[33,34]

External dimensions and porosities of PPF scaffolds are shown in Table 1. No distortions were found in the PPF scaffolds compared to the CAD models. However, they shrank approximately 12% in their length and width compared to CAD models, and the shrinkage was independent of pore sizes. The shrinkage of PPF scaffolds is an inherent characteristic of curing resin and is one of the major drawbacks of stereolithographic fabrication. Resin shrinkage is closely related to the resin type and the width and depth of a solidified line of the resin during curing. Postprocessing and curing can also generate shrinkage as these processes are needed to remove both supports and excess resins inside scaffolds and to solidify partially cured resin.[35,36] This shrinkage can be compensated by measuring dimensions (*x*, *y*, and *z*) of several geometrically scaled rectangular slabs and by determining shrinkage factors from the preprocessing software. To compensate for the shrinkage, we applied percentages of difference in each direction as scaling factors to the stereolithography system and refabricated scaffolds. The resulting scaffolds had external dimensions similar to those of the original CAD models. For example, in the case of scaffolds with a pore size of 913 μm, the measured dimensions were 1.01 ± 0.14 cm (length), 1.00 ± 0.47 cm (width), and 0.30 ± 0.02 cm (height). Furthermore, the height of PPF scaffolds increased as their pore size decreased caused by increased strut thickness in the *z*-axis, which led to decreased porosities of PPF scaffold (Table 2). All porosities of PPF

Table 1. External Dimensions of PPF Scaffolds Compared to CAD Models

pore shape	pore size (μm)	length[b] (cm)	% difference	width[b] (cm)	% difference	height[b] (cm)	% difference
square	913	0.88 ± 0.03*	−11%	0.88 ± 0.02*	−11%	0.30 ± 0.06	0.7%
	778	0.87 ± 0.01*	−12%	0.87 ± 0.06*	−12%	0.30 ± 0.09	1.0%
	670	0.87 ± 0.05*	−12%	0.87 ± 0.05*	−12%	0.31 ± 0.03*	2.3%
	582	0.88 ± 0.04*	−12%	0.87 ± 0.06*	−12%	0.31 ± 0.02*	3.0%
	508	0.88 ± 0.03*	−11%	0.88 ± 0.03*	−12%	0.31 ± 0.05*	4.3%
	446	0.87 ± 0.02*	−12%	0.87 ± 0.02*	−12%	0.32 ± 0.03*	8.3%
hexagon	600[a]	0.89 ± 0.01*	−11%	0.89 ± 0.04*	−11%	0.30 ± 0.09	0.2%

[a] Length of one side. [b] Represents mean ± SD ($n = 5$). * indicates statistically significant difference ($p < 0.05$) between measured dimensions and the CAD models (1.00 cm × 1.00 cm × 0.30 cm).

Table 2. Pore Size and Porosity of PPF Scaffolds Compared to CAD Models

pore shape	pore size (μm)	no. of pores[b] (*xy*-plane)	no. of pores[c] (*z*-axis)	porosity of CAD model (%)	porosity of PPF scaffold[d] (%)	
					gravimetry	micro-CT
square	913	8	2	77.3	64.7 ± 2.0*	61.2 ± 0.4*
	778	9	2	70.8	55.2 ± 1.6*	51.4 ± 0.2*
	670	10	2	67.8	49.1 ± 1.9*	45.3 ± 1.1*
	582	11	3	64.6	47.6 ± 0.3*	44.1 ± 3.4*
	508	12	3	61.4	39.3 ± 1.1*	36.2 ± 2.5*
	446	13	3	55.4	35.2 ± 0.6*	29.9 ± 0.8*
hexagon	600[a]	8	2	79.5	68.7 ± 0.4*	63.5 ± 0.7*

[a] Length of one side. [b] In one row. [c] In one column. [d] Represents mean ± SD ($n = 5$). * indicates statistically significant difference ($p < 0.05$) between measured porosities and the CAD models.

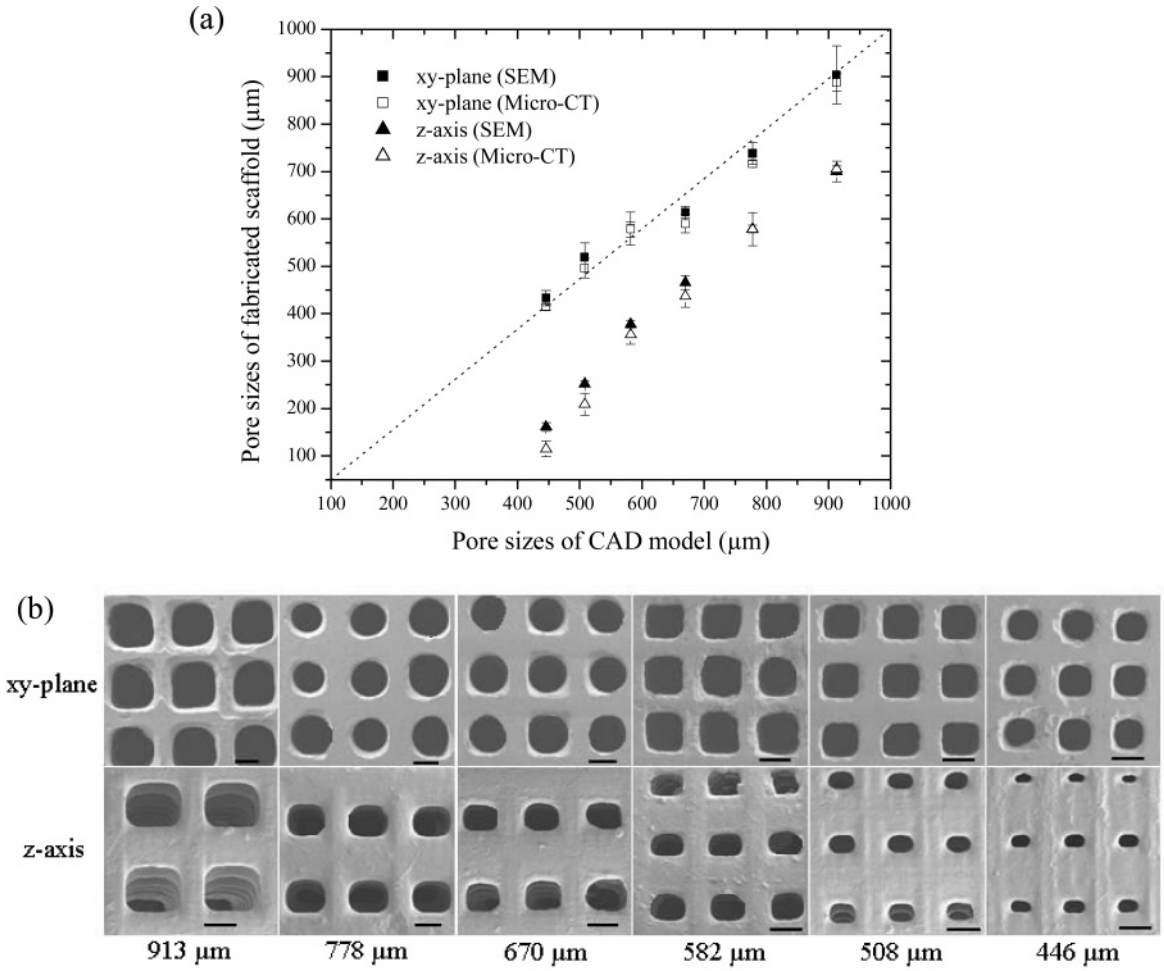

Figure 5. (a) Mean pore sizes of PPF scaffolds compared to CAD models in two directions. The dashed line indicates exact matching between CAD models and fabricated PPF scaffolds. Values represent mean ± SD ($n = 5$). (b) Mean pore sizes of PPF scaffolds with various sized square pores in two directions. Scale bars represent 400 μm.

scaffolds were significantly different from those of CAD models, and porosities of PPF scaffolds from the micro-CT measurements were smaller than those from gravimetry. Since gravimetry used relative density for measuring porosity, it did not distinguish between open and closed pores which led to overestimation of porosity.[37]

From SEM analysis, mean strut thicknesses of PPF scaffolds with square pores increased from 497 ± 16 μm to 737 ± 19 μm as pore size decreased. This result implies that overcuring of resin occurs in small-sized feature remarkably. The deviation between the actual and designed pore size was quite different in the *xy*-plane and *z*-axis. As shown in the inset of Figure 5a, the actual pore sizes from both SEM and micro-CT slices in the *xy*-plane were consistent with the designed values indicated by the dotted diagonal line. In contrast, the actual pore sizes from both methods in the *z*-axis were significantly lower than the designed values and their differences became larger as pore size decreased. While actual pore sizes from micro-CT slices were consistent throughout the slices in the *xy*-plane, those in the *z*-axis were smaller inside the scaffolds than on the surface (data not shown), which was in accordance with decreased porosity as shown in Table 2. This trend could be further evidenced by SEM pictures of those pores in both the *xy*-plane and the *z*-axis in Figure 5b.

Stereolithography could be used to build various 2D patterns and 3D constructs such as hexagon and square pores as shown in Figure 6. SEM pictures of PPF scaffolds with hexagon and square pores show the difference of mean pore sizes between two directions. 3D PPF scaffolds from these designs were successfully fabricated by using PPF/DEF resin and laser

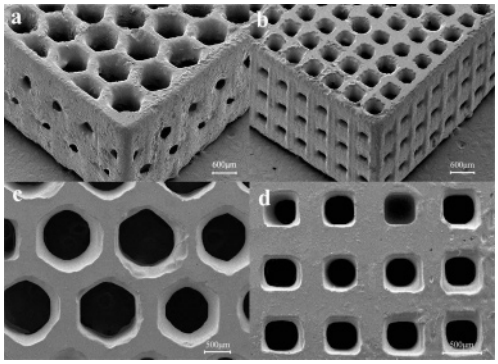

Figure 6. Scanning electron micrographs of PPF scaffolds with (a, c) hexagon and (b, d) square pores. The surfaces shown in c and d are in the *xy*-plane. Length of one side of hexagon pore is 600 μm and square pore size is 508 μm. These values correspond to the scale bars shown in (a, c) and (b, d), respectively.

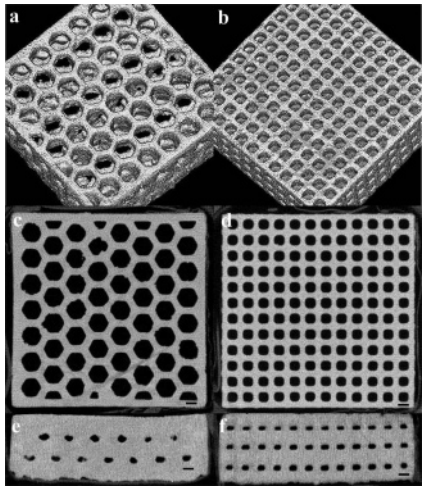

Figure 7. Micro-CT images of PPF scaffolds PPF scaffolds with hexagon (a, c, e) and square pores (b, d, f); 3D volume renderings (a, b), their slices in *xy*-plane (c, d) and *z*-axis (e, f). Length of one side of hexagon pore is 600 μm and square pore size is 508 μm. Scale bars represent 500 μm.

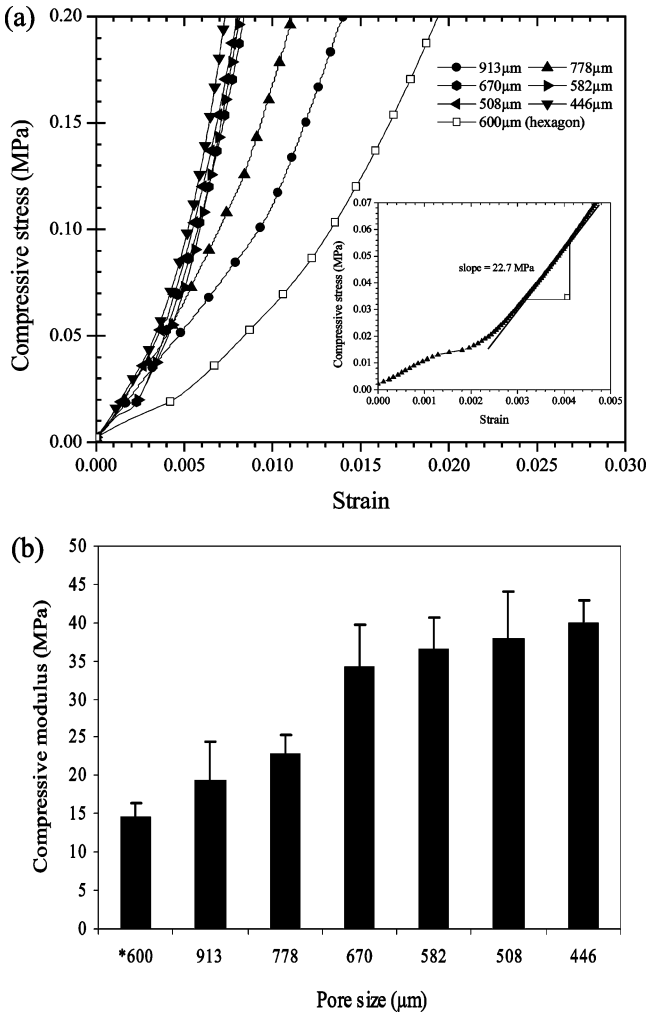

Figure 8. (a) Compressive stress versus strain curve of PPF scaffolds with hexagon and square pores. Inset: Sample calculation of the compressive modulus for the scaffold (pore size = 778 μm). (b) Compressive modulus. *, length of one side of the hexagon pore. Values represent mean ± SD (n = 5).

parameters in stereolithography. Hexagon and square pores in the *z*-axis did not come out as clearly (Figure 6a and 6b) as those in the *xy*-plane (Figure 6c and 6d) because of overcuring of the resin and incomplete removal of excess resins. The square pores were represented more accurately than the hexagon pores in the *z*-axis, although the pore size was small. Since the slice thickness was fixed, this result indicates that the pore geometry is more difficult to be represented accurately in the *z*-axis than for the sides.

Micro-CT images of PPF scaffolds with different pores are shown in Figure 7. Three-dimensional constructs with well-interconnected pores were successfully fabricated by using the determined resin formulations from stereolithography system (Figure 7a and 7b). Pore sizes and geometries of scaffolds with hexagon and square pores were consistent throughout the volume of scaffolds in the *xy*-plane, and there were no pore occlusions inside the scaffolds (Figure 7c and 7d). However, the *z*-axis pore sizes were smaller inside the scaffolds than on the surface as pore size decreased (Figure 7e and 7f), especially for hexagon pores. These results indicate that excess resin was not removed completely inside the scaffolds in the *z*-axis, which led to smaller porosity and pore size of the scaffold.

Figure 8 shows the compression stress versus strain curves and moduli of PPF scaffolds with different pore sizes and shapes. Compression stress increased sharply with decreasing pore size of scaffolds as an exponential pattern in Figure 8a and compressive modulus increased as pore sizes decreased in Figure 8b. However, we could not calculate fracture strength since the maximum force (18 N) of DMA used was not sufficient to break PPF scaffolds. Compression stress versus strain curves were close to each other as pore size decreased. Since we designed CAD models with fixed external dimensions and strut thickness, porosity of scaffold can be determined by pore size (Table 2). In addition to porosity, overcuring of UV curable resin in *z*-axis was obviously seen as pore size decreased, which led to increased *z*-axis dimensions of scaffolds (Table 1). This may be a possible reason for the similar compression modulus of PPF scaffolds with small pore sizes. Moreover, compressive modulus of PPF scaffolds with hexagon pores was smaller than those with square pores of 913 μm because of larger pore size. Since an actual hexagon pore was considered as the maximum diagonal length, mean hexagon pore sizes in *xy*-plane and *z*-axis were 997 ± 55 μm and 712 ± 34 μm, but mean square pore sizes of 913 μm in two directions were 904 ± 61 μm and 700 ± 22 μm.

In summary, we have investigated optimal UV curable polymer resin and laser parameters for the conventional stereolithography machine. PPF/DEF mixtures with three different weight ratios and BAPO contents were characterized by measuring viscosities and thermal properties of the un-cross-

linked solutions and mechanical properties of the cross-linked scaffolds. PPF/DEF mixture with 60:40 weight ratio and 1% BAPO content is considered optimal UV curable resin for both decreased viscosity and increased mechanical properties. Laser parameters of the resin have been determined from the working curve and the relation between laser speed and energy as $E_c = 10$ mJ/cm^2 and $D_p = 3.66$ mil, respectively. After optimizing the PPF/DEF resin and the laser parameters, 3D scaffolds have been fabricated and characterized by measuring external dimensions, porosities, mean pore sizes in two different directions, and compressive moduli. Stereolithography was successfully used to fabricate 3D scaffolds with controlled microstructures, and therefore it is worthwhile to extend this method to other cross-linkable polymeric biomaterials such as polycaprolactone fumarate and polyethylene glycol fumarate.[38] Features in the *xy*-plane were consistently fabricated with the CAD model; however, controlling overcuring of the resin in the *z*-axis is required for increasing feature accuracy. Both in vitro and in vivo biological evaluations of the 3D scaffolds fabricated using stereolithography are needed to further optimize the bone tissue engineering scaffolds with controlled pore size and porosity.

Acknowledgment. This study was funded by the Mayo Foundation and National Institutes of Health (R01 AR45871, R01 EB003060, and R01 EB000305). We thank James A. Gruetzmacher for help with PPF synthesis, Scott I. Gamb for assistance with SEM, and Patricia E. Beighley and Andrew J. Vercnocke for performing micro-CT scanning and image analysis.

References and Notes

(1) Hutmacher, D. W. *Biomaterials* **2000**, *21*, 2529.
(2) Chen, G.; Ushida, T.; Tateishi, T. *Macromol. Biosci.* **2002**, *2*, 67.
(3) Leong, K. F.; Cheah, C. M.; Chua, C. K. *Biomaterials* **2003**, *24*, 2363.
(4) Yang, S. F.; Leong, K. F.; Du, Z. H.; Chua, C. K. *Tissue Eng.* **2002**, *8*, 1.
(5) Hollister, S. J. *Nat. Mater.* **2005**, *4*, 518.
(6) Tsang, V. L.; Bhatia, S. N. *Adv. Drug Delivery Rev.* **2004**, *56*, 1635.
(7) Sodian, R.; Loebe, M.; Hein, A.; Martin, D. P.; Hoerstrup, S. P.; Potapov, E. V.; Hausmann, H.; Lueth, T.; Hetzer, R. *ASAIO J.* **2002**, *48*, 12.
(8) Bibb, R.; Sisias, G. *Rapid Prototyping J.* **2002**, *8*, 25.
(9) Naumann, A.; Aigner, J.; Staudenmaier, R.; Seemann, M.; Bruening, R.; Englmeier, K. H.; Kadegge, G.; Pavesio, A.; Kastenbauer, E.; Berghaus, A. *Eur. Arch. Otorhinolaryngol.* **2003**, *260*, 568.
(10) Harrysson, O. L. A.; Cormier, D. R.; Marcellin-Little, D. F.; Fajal, K. *Rapid Prototyping J.* **2003**, *9*, 37.
(11) Dhariwala, B.; Hunt, E.; Boland, T. *Tissue Eng.* **2004**, *10*, 1316.
(12) Mapili, G.; Lu, Y.; Chen, S.; Roy, K. *J. Biomed. Mater. Res., Part B* **2005**, *75*, 414.
(13) Peter, S. J.; Miller, M. J.; Yasko, A. W.; Yaszemski, M. J.; Mikos, A. G. *J. Biomed. Mater. Res.* **1998**, *43*, 422.
(14) He, S.; Timmer, M. D.; Yaszemski, M. J.; Yasko, A. W.; Engel, P. S.; Mikos, A. G. *Polymer* **2001**, *42*, 1251.
(15) Lewandrowski, K. U.; Gresser, J. D.; Wise, D. L.; White, R. L.; Trantolo, D. J. *Biomaterials* **2000**, *21*, 293.
(16) Lee, K. W.; Wang, S.; Lu, L.; Jabbari, E.; Currier, B. L.; Yaszemski, M. J. *Tissue Eng.* **2006**, *12*, 2801.
(17) Yaszemski, M. J.; Payne, R. G.; Hayes, W. C.; Langer, R. S.; Aufdemorte, T. B.; Mikos, A. G. *Tissue Eng.* **1995**, *1*, 41.
(18) Peter, S. J.; Kim, P.; Yasko, A. W.; Yaszemski, M. J.; Mikos, A. G. *J. Biomed. Mater. Res.* **1999**, *44*, 314.
(19) Fisher, J. P.; Vehof, J. W.; Dean, D.; van der Waerden, J. P.; Holland, T. A.; Mikos, A. G.; Jansen, J. A. *J. Biomed. Mater. Res.* **2002**, *59*, 547.
(20) Cooke, M. N.; Fisher, J. P.; Dean, D.; Rimnac, C.; Mikos, A. G. *J. Biomed. Mater. Res., Part B* **2002**, *64B*. 65.
(21) Fisher, J. P.; Dean, D.; Mikos, A. G. *Biomaterials* **2002**, *23*, 4333.
(22) Kharas, G. B.; Kamenetsky, M.; Simantirakis, J.; Beinnlich, K. C.; Rizzo, A. M. T.; Caywood, G. A.; Watson, K. *J. Appl. Polym. Sci.* **1997**, *66*, 1123.
(23) Wang, S.; Lu, L.; Gruetzmacher, J. A.; Currier, B. L.; Yaszemski, M. J. *Macromolecules* **2005**, *38*, 7358.
(24) Jorgensen, S. M.; Demirkaya, O.; Ritman, E. L. *Am. J. Physiol.* **1998**, *275*, H1103.
(25) Feldkamp, L. A.; Goldstein, S. A.; Parfitt, A. M.; Jesion, G.; Kleerekoper, M. *J. Bone Miner. Res.* **1989**, *4*, 3.
(26) Moore, M. J.; Jabbari, E.; Ritman, E. L.; Lu, L.; Currier, B. L.; Windebank, A. J.; Yaszemski, M. J. *J. Biomed. Mater. Res.* **2004**, *71A*, 258.
(27) Jacobs, P. F. *Rapid Prototyping & Manufacturing: Fundamentals of Stereolithography*; Society of Manufacturing Engineers: Dearborn, MI, 1992.
(28) Cooke, M. N. Ph.D. Dissertation, Case Western Reserve University, OH, 2004.
(29) Wang, S.; Lu, L.; Yaszemski, M. J. *Biomacromolecules* **2006**, *7*, 1976.
(30) Wang, S.; Wang, S. Q.; Halasa, A.; Hsu, W. L. *Macromolecules* **2003**, *36*, 5355.
(31) Wang, S.; von Meerwall, E. D.; Wang, S. Q.; Halasa, A.; Hsu, W. L.; Zhou, J. P.; Quirk, R. P. *Macromolecules* **2004**, *37*, 1641.
(32) Murugan, R.; Ramakrishna, S. *Compos. Sci. Technol.* **2005**, *65*, 2385.
(33) Gauthier, O.; Bouler, J. M.; Aguado, E.; Pilet, P.; Daculsi, G. *Biomaterials* **1998**, *19*, 133.
(34) Karageorgiou, V.; Kaplan, D. *Biomaterials* **2005**, *26*, 5474.
(35) Hutmacher, D. W.; Sittinger, M.; Risbud, M. V. *Trends Biotechnol.* **2004**, *22*, 354.
(36) Wang, W. L.; Cheah, C. M.; Fuh, J. Y. H.; Lu, L. *Mater. Des.* **1996**, *17*, 205.
(37) Karande, T. S.; Ong, J. L.; Agrawal, C. M. *Ann. Biomed. Eng.* **2004**, *32*, 1728.
(38) Wang, S.; Lu, L.; Gruetzmacher, J. A.; Currier, B. L.; Yaszemski, M. J. *Biomaterials* **2006**, *27*, 832.

BM060834V